GENERATION OF INTERNAL GRAVITY WAVES BY A KATABATIC WIND IN AN IDEALIZED ALPINE VALLEY

Charles Chemel[1,2], Chantal Staquet[1] & Yann Largeron[1]

[1] Laboratoire des Ecoulements Géophysiques et Industriels, CNRS / UJF / INPG, Grenoble, France
[2] Centre for Atmospheric & Instrumentation Research, University of Herfordshire, Hatfield, United Kingdom
E-mail: Chantal.Staquet@legi.inpg.fr

Submitted to Meteorology and Atmospheric Physics, 22 october 2008 (revised version)

Abstract: The dynamics of the atmospheric boundary layer in an alpine valley at night or in winter is dominated by katabatic (or down-slope) flows. As predicted by McNider (1982) oscillations along the slope are expected to occur if the fluid is stably-stratified, as a result of buoyancy and adiabatic cooling/warming effects. Internal gravity waves must also be generated by the katabatic flows because of the stable stratification. The aim of the present paper is to identify and characterize the oscillations in the katabatic flow as well as the internal gravity wave field emitted by this flow. Numerical simulations with the ARPS code are performed for this purpose, for an idealized configuration of the Chamonix valley. We show that the oscillations near the slope are non propagating motions, whose period is well predicted by the single particle model of McNider (1982) and equal to 10 to 11 mn. As for the wave field, its frequency is close to $0.85N$, where N is the value of the Brunt-Väisälä frequency in the generation region of the waves, consistently with previous academic studies of wave emission by turbulent motions in a stratified fluid. This leads to a wave period of 7 to 8 mn.

Keywords: ICAM 2007, stably-stratified atmosphere, alpine valley, katabatic winds, temporal oscillations, internal gravity waves, numerical simulations, ARPS code.

1. INTRODUCTION

As soon as the ground surface is not flat, a horizontal temperature gradient is created at night between the air adjacent to that surface and the ambient air because of radiative cooling of the ground. A katabatic (i.e. downslope) flow is thereby induced. This flow is a gravity current, namely a jet of cold air confined near the ground. Katabatic flows are well-known to develop along gentle slopes of ice shelfs (e.g. Derbyshire & Wood (1994), Renfrew (2004)). For steep slopes (larger than about 10 degrees), the features of katabatic flows have also been well documented through *in situ* measurements, laboratory experiments or numerical simulations either on a simple slope (f.i. Helmis & Papadopoulos (1996), Monti et al. (2002), Skyllingstad (2003), Baines (2005)) or in a valley (Gryning et al. (1985), van Gorsel et al. (2004)): the along-slope velocity is of a few meters per second with a high shear, whose maximum value is reached at a few tens of meters above the ground, depending upon the distance from the top of the slope.

As predicted by Fleagle (1950) from particle dynamics, oscillations of the katabatic flow are expected because of compressible warming and radiative cooling of the ground. When the atmosphere is stable, McNider (1982) showed that the oscillations are further contributed by the restoring buoyancy force. Such oscillations have been reported in several papers from measurements near the slope (Gryning et al. (1985), Helmis & Papadopoulos (1996), van Gorsel et al. (2004), Monti et al. (2002), Bastin & Drobinski (2005)). The oscillating katabatic flow should emit internal gravity waves when the atmosphere is stable[1], as was also reported in field measurements (van Gorsel et al. (2004), Mori & Kobayashi (1996), Whiteman et al. (2008)). However, no systematic study of this

[1]These waves should be made distinct from lee waves which result from the interaction of a wind with a topography.

wave field has been performed and this is the main purpose of the present paper: our aim is to identify and characterize the oscillations in the katabatic flow as well as the internal gravity wave field emitted by this flow. The topography of an alpine valley under stable atmospheric conditions will be considered. This configuration may be considered as highly idealized since a mixed residual layer often exists in the valley at night or in winter and the stratification is partly produced by the katabatic flow itself (Mori & Kobayashi (1996)). However, stable vertical temperature profiles can be extracted from field measurements and we shall use such a realistic profile to initialize our temperature field.

Several questions are currently unanswered : do the oscillations pertain to the wave field? What are the wave characteristics? What does happen to the waves once emitted? To address these questions, we analyse numerical simulations performed with the ARPS code. The simulations are described in the next Section. The characteristics of the oscillating and wave fields are reported in Section 3 and conclusions are drawn in the final Section.

2. METHODOLOGY

The simulations employ the ARPS code (Advanced Regional Prediction System, Xue et al. (2000)) for an idealized configuration of the Chamonix valley. The valley is oriented along the NS axis and is opened at one boundary to allow for the development of an along-valley wind. The analytic expression of the topography is provided in Rampanelli et al. (2004). The geometry of the valley is displayed in Figure 1a. Its length is 20 km while its width is 1240 m at bottom level, located at sea level. The sloping sidewall width (which comes into play in the definition of the topography) is equal to 2640 m. Summits at altitude 1700 m dominate the bottom of the valley. The altitude of the summits actually varies along the valley axis, as shown in Figure 1b, the altitude of 1700 m being reached at the North end of that axis. The maximum value of the slope angle varies as well along the valley axis and, hereafter, we use a mean value of 35^o for this angle.

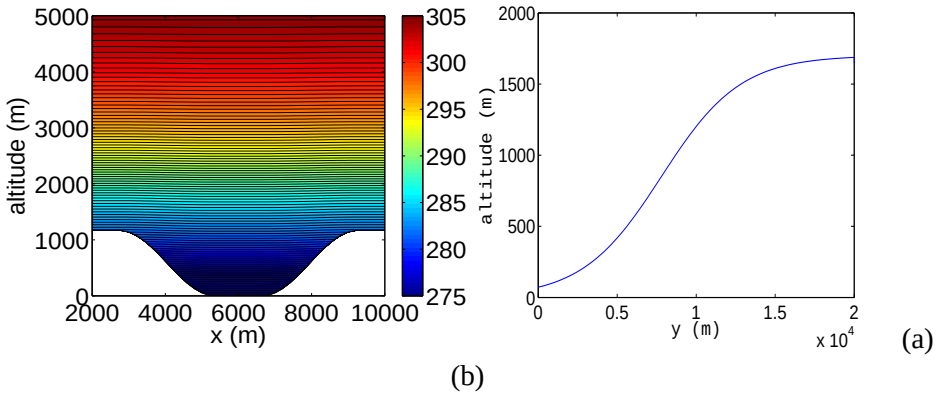

Figure 1: (a) Constant contours of the initial potential temperature field (in K) in the mid-plane perpendicular to the valley axis. The geometry of the valley is also displayed. (b) Vertical cross-section (at $x = 2$ km) of the topography along the valley axis, showing how the altitude of the summits changes along that axis (note the difference of scale between the two coordinate axes).

The simulations model a winter situation for which a 3^o difference exists between the ground surface and the air just above it (the ground surface being colder than the air). The initial time of the computation is 2200 UTC, on Decembre 21st, at the latitude of the Chamonix valley. The horizontal temperature difference between the air adjacent to the ground surface and the ambient air creates a pressure gradient which triggers the katabatic flow. No velocity field is imposed at initial time.

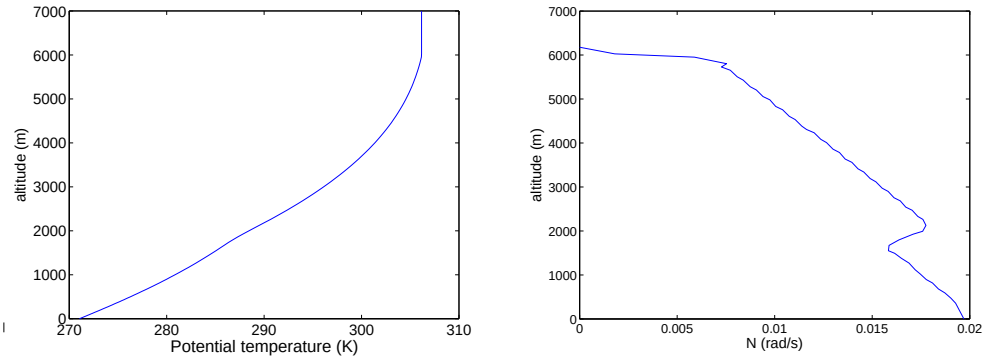

(a) (b)

Figure 2: (a) Initial potential temperature profile; the potential temperature field is uniform in the horizontal plane. (b) Corresponding Brunt-Väisälä frequency.

The air is stably-stratified, with an initial temperature profile inferred from measurements during the MAP-Riviera campaign (Tavernier (2006)). This profile is displayed in Figure 2 along with the corresponding Brunt-Väisälä frequency N. Constant contours of the initial temperature field are also visible in Figure 1a. We recall that N is defined by $N^2 = g/T_0 \; d\theta/dz$, where T_0 is a temperature reference equal here to 271K, namely to the temperature at ground level at the beginning of the computation, and θ is the potential temperature field.

Open boundary conditions are used in the NS and EW directions and a Rayleigh sponge absorbs motions reaching the top of the domain. The horizontal resolution is 200 m both in the $x-$ and $y-$directions. A variable grid is used along the vertical direction, the resolution being 5 m near the ground level and slowly increasing upwards. The corresponding resolution is 61x103x140 grid points.

3. ANALYSIS OF THE OSCILLATING AND INTERNAL GRAVITY WAVE FIELDS

3.1 Background

The oscillations of the katabatic flow are well predicted by the model of McNider (1982) for a fluid particle flowing down along a slope of constant value α in a stably-stratified atmosphere with constant N. The fluid particle is subjected both to adiabatic warming and to a restoring buoyancy force, since the medium is stably-stratified, which decelerate the particle. Radiative cooling from the ground then cools the slowly moving particle, which accelerates, and the cycle is repeated. These mechanisms lead to temporal oscillations of the velocity of the fluid particle at frequency $\omega = N\sin\alpha$ about a mean value which depends upon the cooling rate.

The unsteadiness of the katabatic flow resulting from this oscillating process (and from possible dynamical instabilities of this flow) perturbs the stably-stratified fluid. As a result, internal gravity waves should be emitted from the slope and propagate away from it. It is well-known that a bounded object oscillating at a fixed frequency Ω in an infinite stably-stratified fluid with constant N emits internal gravity waves at the same frequency whose energy propagates at a given angle θ to the vertical. The angle θ is imposed by the dispersion relation, which is expressed as, ignoring Coriolis effects:

$$\Omega^2 = N^2 \cos^2\theta. \tag{1}$$

(*f.i.* Lighthill (1978)). Voisin (2007) showed theoretically that, when N is fixed and Ω varies from 0 to its upper bound N, the power of the waves radiated by an oscillating sphere is maximum for $\Omega/N \simeq 0.84$ (and for $\simeq 0.82$ for an oscillating cylinder). These results have been verified experimentally

(Ermanyuk & Gavrilov (2003)). Interestingly, when a mixed region is released at its equilibrium level (Wu (1969)) or above it (Cerasoli (1978)), in a constant N stratified fluid, the power spectrum of the radiated waves is peaked at a frequency Ω such that $\Omega/N \simeq 0.8$ as well.

From these results, it follows that two systems of oscillations are expected in the stably-stratified atmospheric boundary layer of a valley: (i) a system of temporal oscillations located near the slope at frequency ω such that $\omega/N = \sin\alpha$ and (ii) a system of propagating motions, consisting of the internal gravity wave field, propagating from the slope and away from it at frequency $\Omega/N \simeq 0.8$. Since the temporal oscillations along the slope have been inferred from particle dynamics, no phase propagation (that is, no wave motion) is assumed, which will need to be checked.

3.2 Oscillations along the slope

Figure 3 provides an overview of the flow field in a vertical plane at 2230 UTC, by displaying the horizontal (along x) and vertical components of the velocity field in frames (a) and (b) respectively. The flow is nearly symmetric about the mid-plane of the valley because of the symmetry of the topography and of the initial condition. The largest values of u (frame (a)) are reached along the slope, within the downslope flow, and are close to ± 6 m/s; for comparison, the minimum vertical velocity is close to -2.8 m/s. These values are consistent with those obtained from *in situ* measurements. In order to visualize the lower amplitude internal gravity wave field, a limited range of w values are displayed in frame (b). The features of this field are discussed in the next Section.

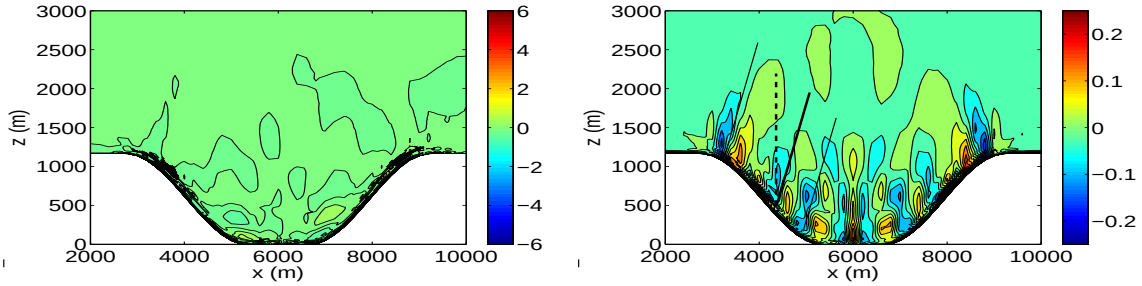

Figure 3: Constant contours of components of the velocity field (in m/s) in the mid-plane perpendicular to the valley axis, at 2230 UTC. (a) Component along the x-axis. (b) Vertical component; a limited range of values is selected for a clear visualization of the wave field. The inclined full lines mark the slope of the phase lines; the angle between the vertical dashed line and the inclined bold full line is about 30^o.

No clear information can be obtained from Figure 3a about the occurence of oscillations in the katabatic flow and a detailed analysis of the frequency content of the velocity field close to the slope is now presented. These oscillations occur if the slope is long enough. Indeed, from McNider's model, the velocity field along the slope is of the form U_0(1-cos($N\sin\alpha\ t$)), ignoring friction; the displacement amplitude scales therefore like $U_0(t-\sin(N\sin\alpha\ t)/(N\sin\alpha))$. With U_0 of the order of 5 m/s, $N \simeq 0.018$ rad/s and $\alpha = 35^o$, this yields an excursion of the fluid particles of 1000 m already after 5 mn. Hence, oscillations at frequency $N\sin\alpha = 0.01$ rad/s should be best detected near the North end of the valley, where the slopes are the longest, and close to the valley axis.

We therefore computed the frequency spectrum of one velocity component (w here), near the bottom of the slope, at $x = 4.4$ km, for different values of y larger than 16 km. Results are displayed in Figure 4. Since N is not exactly constant and the slope varies, deviations from this theoretical prediction may occur. All spectra nevertheless exhibit a peak around 0.01 rad/s, which is the expected oscillating frequency. The values of these peaks are $\omega = 0.0105$ rad/s for frame a) and $\omega = 0.0093$

rad/s for frames b) and c), corresponding to an oscillating period $T = 2\pi/\omega$ ranging between 10 and 11 mn. Figure 4 also shows that other maxima are reached at a higher frequency, around 0.015 rad/s, which should be attributed to the presence of internal gravity waves as we shall see.

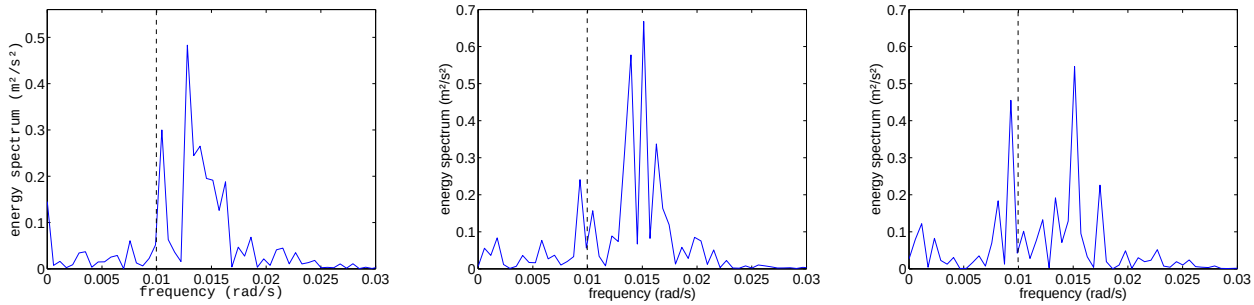

(a) (b) (c)

Figure 4: Frequency spectrum of the vertical velocity at the bottom of the slope ($x = 4.4$ km), 50 m above the slope for different locations along the valley axis: (a) $y = 15.6$ km, (b) $y = 16.6$ km, $y = 19.6$ km. The vertical line indicates the oscillating frequency $N\sin\alpha$ predicted by McNider's model (with $N = 0.018$ rad/s and $\alpha = 35^o$).

The spectrum does not allow one to determine whether the peak frequency around 0.01 rad/s is associated with propagating or non-propagating motions. To investigate this point, we should normally filter the data around this frequency before performing any analysis. We show below that this is not necessary if the signal at the oscillating frequency is strong enough with respect to the other frequencies. A Hövmoller diagram in (z,t) coordinates is thus plotted for the vertical velocity in Figure 5a. This diagram simply displays w along a vertical line as a function of time. The slope of the phase lines in this diagram is equal to the phase velocity along the z-direction namely $dz/dt = c_z$. The z-component of the wave vector of the propagating motions (assumed to be spatially monochromatic), denoted k_z, can be inferred from this computation since $k_z = \omega/c_z$. For instance, vertical phase lines yield $k_z = 0$ implying that there is no propagation along the vertical direction.

Figure 5a shows that, near the ground, at all times, the phase lines are precisely vertical over a height of about 30 m. Hence, oscillating motions without vertical phase propagation occur near the slope. In other words, k_z may be assumed to be zero near the slope.

A Hovmöller diagram in (y,t) coordinates is displayed in Figure 5b. The slope of the phase lines is vertical again during the first 40 mn or so; though the pattern becomes more complicated later on, no clear inclination can be detected after this time. Hence we may assume that $k_y = 0$ as well. It follows that $k_x = 0$ also since a non zero value of k_x would be associated with a propagating motion along the x-direction only, which is unphysical. It can thus be concluded that the oscillations along the ground with frequency $N\sin\alpha$ are associated with temporal oscillations only that is, there is no phase propagation. (Therefore, these oscillations should not be interpreted as internal gravity waves propagating normal to the slope, as a formal analogy with the dispersion relation would suggest it, using $N\sin\alpha = N\cos(\pi/2 - \alpha)$.)

3.3 Kinematics of the emitted wave field

Figure 3b shows that vertical velocity contours of alternate sign emanate from the katabatic flow, thereby attesting of the emission of internal gravity waves. These waves are emitted all along the slope, with phase lines making nearly the same angle with the vertical whatever the slope angle at the emission location. From the dispersion relation (1), this implies that the waves are monochromatic in

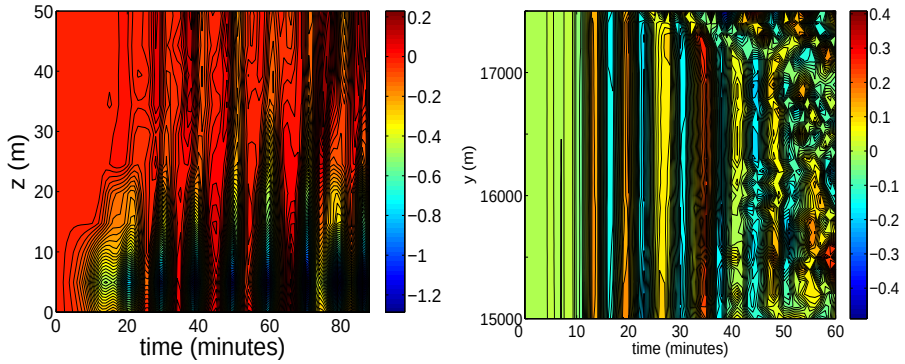

(a) (b)

Figure 5: (a) Hovmöller diagram of the vertical velocity (in m/s) : (a) in (z,t) coordinates along the line defined by $x = 5.2$ km and $y = 15$ km. (b) in (y,t) coordinates along the line defined by $x = 4.4$ km and $z = 500$ m (200 m above topography), for y larger than 15 km.

time. In the center of the valley, the phase lines are nearly vertical because waves with nearly opposite horizontal phase velocity superimpose (hence standing waves are created there).

The purpose of this section is to determine the frequency Ω of the internal gravity wave field emitted by the unsteady katabatic flow and, if the wave field appears to be monochromatic in space as well, its wave vector $\vec{k}$. The spatial monochromaticity is not obvious. Indeed, the dispersion relation shows that the angle of the wave vector is selected by Ω and N, but not its modulus $|\vec{k}|$. Hence, any scale $1/|\vec{k}|$ such that $\vec{k}$ makes the angle θ with the vertical may *a priori* be generated. In practice, a definite length scale appears, which is selected by the size of the source which emits the waves for instance (see, e.g., Staquet & Sommeria (2002)).

3.3.1 Frequency of the emitted wave field

The frequency Ω will be determined from three independent methods: (i) from the peak of the frequency spectrum of the vertical velocity at a point well above the topography; (ii) from the angle of the phase lines with the vertical; (iii) from Hovmöller diagrams at high altitude. The second and third methods are strictly valid when N is constant, since they rely upon the dispersion relation (1) which has been derived under that assumption. As shown in Figure 2b N changes by not more than 20% over the first 1700 m above sea level, where the waves are generated. We shall therefore assume that the dispersion relation remains valid and use a constant value for N.

The frequency spectrum of the vertical velocity is plotted in Figure 6 in the mid-plane along the valley axis at two locations mainly differing by their altitude. Both spectra display a well-defined peak, at a frequency close to 0.015 rad/s: $\Omega = 0.0145$ rad/s for frame a) and $\Omega = 0.0156$ rad/s for frame b). The corresponding periods are 433 s and 403 s respectively. With $N = 0.017$ rad/s (which is the value of N at the generation region of the waves, at $z \simeq 1100$ m), this leads to $\Omega/N = 0.85$ and $\Omega/N = 0.92$ respectively. The former value is in good agreement with the values found in the literature, as discussed in the Introduction, while the latter is slightly higher.

The second method consists in computing the slope of the phase lines displayed in Figure 3b. The straight lines drawn in Figure 3 are all parallel, showing that a definite value for the angle of the phase lines can be inferred. The lines plotted correspond to $\theta = 30^o$, namely to $\Omega/N \simeq 0.87$. With $N = 0.017$ rad/s, one gets $\Omega = 0.0147$ rad/s leading to a wave period equal to 427 s. All these values are totally consistent with those found from the first method.

Hence the waves have a period of about 7 mn. This is confirmed by the computation of the

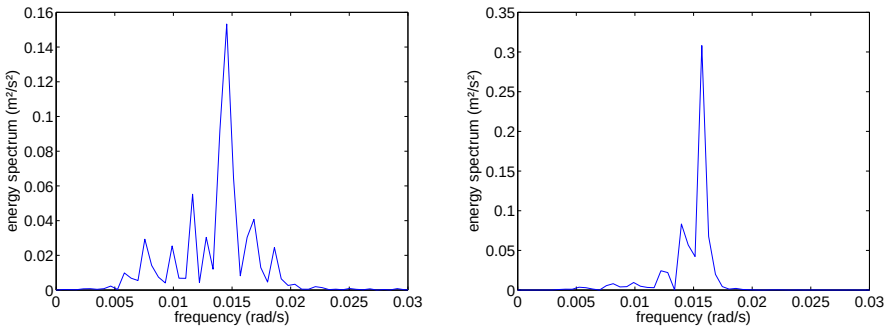

(a) (b)

Figure 6: Frequency spectrum of the vertical velocity in the mid-plane along the valley axis (a) at $x = 3$ km and $z = 1500$ m (400 m above topography); (b) at $x = 3.4$ km and $z = 2200$ m (1300 m above topography).

Hovmöller diagrams as we show it now.

3.3.2 Wavelengths of the emitted wave field

Hovmöller diagrams show that free waves propagate from $z \simeq 2200$ m and up. Below that altitude, such as $z = 1500$ m, confinement effects by the valley slopes lead to a standing wave system from $t \simeq 50$ mn. We thus analyse the Hovmöller diagrams for $z = 2200$ m.

The (y,t) Hovmöller diagram is displayed in Figure 7a over the whole length of the valley and for one hour. A striking feature is that two wave packets are actually generated, about the mid-plane along the valley axis and close to the North end of the valley. We focus on the former wave system in the following. The phase lines are close to the vertical for this wave packet implying that the waves propagate in a vertical plane perpendicular to the valley axis. Hence, only k_x and k_z need to be determined.

Due to the symmetry of the wave pattern, only half of the domain along the x-direction is plotted in the (x,t) diagram (Figure 7b). The phase lines display a well-defined slope, which slightly varies as time elapses. Since the medium changes only in the z-direction (because N varies along the vertical), the frequency Ω and k_x are unchanged. Hence $c_x = dx/dt$ should not change with time if the waves were freely propagating. The interaction between wave packets emitted from either slope of the valley may be responsible for this change. At early times (before $t = 50$ mn), the diagram yields $c_x = 3.3$ m/s.

The same analysis can be performed from the (z,t) diagram, displayed in Figure 7c. The diagram clearly shows that the wave packet is emitted from the ground and propagates upwards -as attested by the inclined phase lines leaving the ground as time elapses- while vertical structures -namely the oscillations discussed in the previous section- are left on the ground. The slope of the inclined phase lines is negative, consistently with internal gravity wave kinematics. Indeed the vertical component of the group velocity and of the phase velocity have opposite signs (for a positive frequency) (Lighthill (1978)). Since the former component is positive, as the waves are emitted upwards from the ground, the latter component is expected to be negative. We found $c_z = -4.4$ m/s.

Assuming N is constant, the dispersion relation can be invoked again to infer a value for Ω/N from those of the phase velocities. Indeed, this relation can also be written (assuming Ω is positive):

$$\frac{\Omega}{N} = \left(1 + \frac{c_x^2}{c_z^2}\right)^{-1/2}. \qquad (2)$$

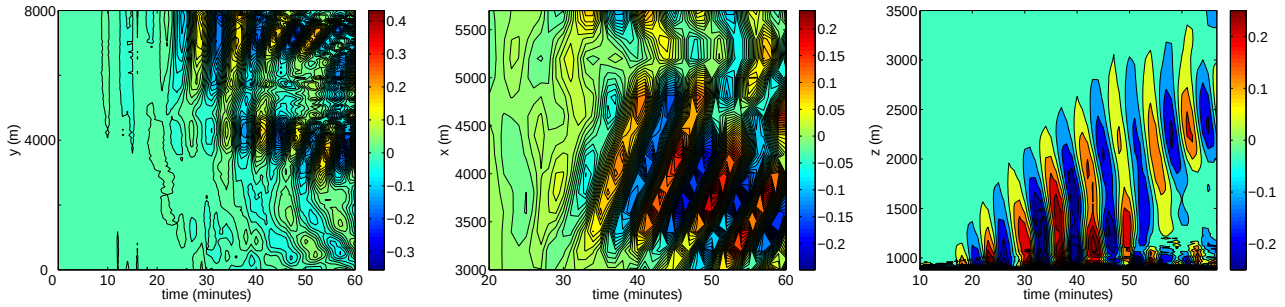

(a) (b) (c)

Figure 7: Hovmöller diagrams of the vertical velocity: (a) in a (y,t) plane, for $x = 3.4$ km and $z = 2200$ m (1300 m above topography); (b) in a (x,t) plane, for $y = 9.8$ km and $z = 2200$ m; (c) in a (z,t) plane, for $x = 3.4$ km and $y = 9.8$ km.

Using the values of c_x and c_z, one gets $\Omega/N \simeq 0.80$, which is consistent with our finding from the direct measurement of the angle of the phase lines from Figure 3.

The finding of two well-defined values for the phase velocity along the x- and z-directions imply that the wave field has a well-defined length scale along the x and z directions as well. These length scales are obtained in a straightforward manner. Using $\lambda_x = 2\pi.c_x/\Omega$, we find $\lambda_x \simeq 1500$ m (using $\Omega/N \simeq 0.80$ and $N = 0.017$ rad/s). As well, we get $\lambda_z \simeq 2000$ m.

The scale which sets the value for λ_x is not clear yet. This value is close to the width of the valley, which suggests that the horizontal extent of the valley may set it. However, we ran a simulation being identical to the one analysed in the present paper except for the bottom width of the valley, which was doubled (being set to 2480 m). The analysis of the (x,t) Hovmöller diagram for this simulation led to the same estimate for λ_x, namely $\lambda_x \simeq 1300$m. As for the vertical wavelength λ_z, it is completely determined from the dispersion relation once Ω, N and k_x are known. We just note that λ_z is of the same order as the highest altitude of the summits.

Hence large scale internal gravity waves are emitted from the slope.

4. CONCLUSION

This academic study dealt with the atmospheric boundary layer under stable conditions in an alpine valley. An idealized topography was considered, as a model of the Chamonix valley. We focused upon the along-slope oscillations and upon the internal gravity wave field generated by the unsteady katabatic flow. We showed that these two oscillating systems are distinct but have close periods in the present context of steep slopes. The oscillations, which are well-predicted by the single particle model of McNider (1982), are not associated with any phase propagation and have a period of 10 to 11 mn. The frequency Ω of the waves is such that, assuming the Brunt-Väisälä frequency varies weakly enough in space so that the dispersion relation may be assumed to be valid, $\Omega/N \simeq 0.8 - 0.9$, consistently with previous works on internal wave emission by oscillating objects and turbulent fluids. The corresponding wave period is 7 to 8 mn.

The internal wave field appears to be organized into two wave packets, which propagate in a vertical plane perpendicular to the valley axis. These two planes are located at mid-distance along the valley axis and at its end part, where the slopes are the longest. The waves have large wavelengths, of the same order as the dimensions of the valley, but we could not conclude at the scales which set these wavelengths. Indeed only a time scale (but no length scale) is imposed for internal gravity waves, which is N^{-1}.

As time elapses, the wave packets become trapped below a reflecting level, due to the change in the Brunt-Väisälä frequency with altitude. As a result, velocity and temperature fluctuations arise everywhere between that level and the valley floor, implying that turbulence and, possibly, mixing may occur. This point is under investigation, as is also the application of the present analysis to the realistic configuration of the Grenoble valley.

ACKNOWLEDGMENTS

This work benefitted from fruitful discussions with Bruno Voisin. Financial support from the 2007 IDAO/LEFE program of INSU is greatly acknowledged.

REFERENCES

Baines P.G. 2005: Mixing regimes for the flow of dense fluid down slopes into stratified environments. *J. Fluid Mech.*, **538**, 25-267.

Bastin S. and Drobinski P. 2005: Temperature And Wind Velocity Oscillations Along a Gentle Slope During Sea-Breeze Events. *Boundary-Layer Meteorology*, **114**(3): 573.

Cerasoli C.P. 1978: Experiments on buoyant-parcel motion and the generation of internal gravity waves, *J. Fluid Mech.*, **86**, 247–271.

Derbyshire S.H. and Wood N. 1994: The sensitivity of stable boundary layers to small slopes and other influences. In I.P. Castro and N.J. Rockliff (eds), Stably stratified flows : flow and dispersion over topography, pp, 105118, Clarendon Press, Oxford

Ermanyuk E.V. and Gavrilov N.V. (2003): Force on a body in a continuously stratified fluid. Part 2. Sphere, *J. Fluid Mech.*, **494**, 33–50.

Fleagle R.G. (1950): A theory of air drainage. *J. Meteorology*, **7**, 227-232.

van Gorsel E., Vogt R., Christen A. and Rotach M. 2004: Low frequency temperature and velocity oscillations in katabatic winds. *International Conference on Alpine Meteorology*, Brig, May 19 to 23, 2003.

Gryning S.-E., Mahrt L. and Larsen S. 1985: Oscillating nocturnal slope flow in a coastal valley, *Tellus*, **37**A, 196-203.

Helmis C.G. and Papadopoulos K.H. 1986: Some aspects of the variation with time of katabatic flow over simple slope, *Quart. J. Roy. Meteor. Soc.*, **122**, 595-610.

Lighthill J. 1978: Waves in Fluids (Cambridge University Press, 1978).

McNider R.T. 1982: A note on velocity fluctuations in drainage flows. *J. Atmos. Sci.*, **39** (7), 1658-1660.

Monti P., Fernando H.J.S., Princevac M., Chan W.C., Kowalewski T.A. and Pardyjak E.R. 2002: Observations of flow and turbulence in the nocturnal boundary layer over a slope. *J. Atmos. Sci.*, **59**, 2513–2534.

Mori M. and Kobayashi T. 1996: Dynamic interaction between observed nocturnal drainage winds and a cold air lake. *J. Meteorol. Soc. Japan.*, **74**-2, 247–258.

Rampanelli G., Zardi D. and Rotunno R. (2004): Mechanism of up-valley winds. *J. Atmos. Sci.*, **61**, 3097-3111.

Renfrew I.A. (2004): The dynamics of idealized katabatic flow over a moderate slope and ice shelf. *Quart. J. Roy. Meteor. Soc.*, **130 (A)**, 1023-1045.

Skyllingstad E.D. (2003): Large eddy simulations of katabatic flows. *Boundary Layer Met.*, **106**, 217-243.

Staquet C. and Sommeria J. 2002: Internal gravity waves: from instabilities to turbulence, *Annual Reviews in Fluid Mechanics*, **34**, 559-593.

Tavernier M. 2006: Investigation numérique des ondes internes en vallée encaissée : mécanisme de génération et mélange induit. *Rapport de stage de Master*, Université Joseph Fourier.

Voisin B. 2007: Added mass effects on internal wave generation. *Fifth International Symposium on Environmental Hydraulics*, Tempe, AZ, USA, 4–7 decembre 2007.

Wu J. 1969: Mixed region collapse with internal wave generation in a density-stratified medium, *J. Fluid Mech.*, **35**, 531–544.

Whiteman D.C. et al. 2008: METCRAX 2006: Meteorological Experiments in Arizona's Meteor Crater, *Bull. Amer. Meteor. Soc.*, submitted.

M. Xue, Droegemeier K. K. and Wong V. 2000: The Advanced Regional Prediction System (ARPS) – A multi-scale non hydrostatic atmospheric simulation and prediction model. Part I: Model dynamics and verification, *MAP*, **75**,161-193.